Overview of NIST Activities on Sub-size and Miniaturized Charpy Specimens: Correlations with Full-Size Specimens and Verification Specimens for Small-Scale Pendulum Machines[1]

Enrico Lucon[2]
National Institute of Standards and Technology
Applied Chemicals and Materials Division
325 Broadway, Boulder CO 80305 (USA)
enrico.lucon@nist.gov

Chris N. McCowan
National Institute of Standards and Technology
Applied Chemicals and Materials Division
325 Broadway, Boulder CO 80305 (USA)
chrismccowan81@gmail.com

Raymond L. Santoyo
National Institute of Standards and Technology
Applied Chemicals and Materials Division
325 Broadway, Boulder CO 80305 (USA)
raymond.santoyo@nist.gov

ABSTRACT

NIST in Boulder Colorado investigated the correlations between impact test results obtained from standard, full-size Charpy specimens (CVN) and specimens with reduced thickness (sub-size Charpy specimens, SCVN) or reduced or scaled cross-section dimensions (miniaturized Charpy specimens, MCVN). A database of instrumented impact test results was generated from four line pipe steels, two quenched

[1] Contribution of NIST, an agency of the US government; not subject to copyright in the United States.
[2] Corresponding author.

and tempered alloy steels, and an 18 Ni maraging steel. Correlations between specimen types were established and compared with previously published relationships, considering absorbed energy, ductile-to-brittle transition temperature, and upper shelf energy. Acceptable correlations were found for the different parameters, even though the uncertainty of predictions appears exacerbated by the expected significant experimental scatter. Furthermore, we report on the development of MCVN specimens for the indirect verification of small-scale pendulum machines (with potential energies between 15 J and 50 J), which cannot be verified with full-size verification specimens. Small-scale pendulum machines can now be verified at room temperature with certified reference specimens of KLST type (3 mm × 4 mm × 27 mm), supplied by NIST at three certified absorbed energy levels (low energy, 1.59 J; high-energy, 5.64 J; super-high energy, 10.05 J). These specimens can also be used to verify the performance of instrumented Charpy strikers through certified maximum force values. Certified reference values for both absorbed energy and maximum force were established by means of an interlaboratory comparison (Round-Robin), which involved nine qualified and experienced international laboratories.

INTRODUCTION

Charpy V-notch testing is extensively used in the industry for ensuring that materials exhibit adequate toughness and resistance to brittle fracture. Typically, specifications require that a certain level of absorbed energy be achieved at a specified test temperature (either room temperature, or minimum design temperature).

A practical difficulty is encountered for small section thicknesses, or components with complicated shapes, when standard full-size Charpy V-notch specimens (CVN) cannot be extracted. Under these circumstances, Charpy specimens with reduced

thicknesses[3] are typically machined and tested. Typical thickness values for sub-size Charpy specimens (SCVN) are 7.5 mm (3/4-size), 6.67 mm (2/3-size), 5 mm (1/2-size), and 2.5 mm (1/4-size). An alternative approach is to reduce both cross section dimensions (thickness and width), rather than just the thickness, as well as the remaining dimensions: in this case, specimens are denominated miniaturized Charpy-V notch (MCVN). The most popular MCVN specimen type is designated KLST (from the German *Kleinstprobe*), and has thickness B = 3 mm, width W = 4 mm, notch depth N = 1 mm and length L = 27 mm. Another MCVN specimen configuration considered in this study is designated RHS (*Reduced Half-Size*), and has $B = W$ = 4.83 mm, N = 0.97 mm, and L = 24.13 mm. The main difference between KLST and RHS is that only the latter is proportionally scaled with respect to CVN.

Although it would seem logical that a Charpy specimen with reduced cross-section would absorb less energy than a full-size CVN and that energy reduction should be proportional to the reduction in the area of the remaining ligament below the notch, the situation is more complex for ferritic steels. The reduction in specimen thickness (and also specimen width for MCVN specimens) causes a loss in through-thickness constraint, leading to a decrease in the ductile-to-brittle transition temperature. Therefore, in order to correlate the results obtained from CVN and SCVN/MCVN specimens, one needs to both account for the transition temperature shift and factor the absorbed energy by an amount appropriate to the reduced cross-sectional area. This

[3] In this paper, we will call "thickness" (B) the dimension parallel to the machined notch, in accordance with fracture mechanics terminology. In current Charpy standards, this dimension is referred to as specimen width (W).

approach is generally adopted by North American standards, while European standards tend to require a higher absorbed energy per unit cross-sectional area (absorbed energy density) for a SCVN/MCVN specimen tested at the same temperature [1].

The study presented here attempts to correlate Charpy results obtained from CVN, SCVN, and MCVN specimens of seven ferritic steels tested at NIST in Boulder Colorado. The results will be compared to previously published correlations.

MATERIALS AND EXPERIMENTAL

Among the seven ferritic steels characterized at NIST, four were commercial line pipe steels (X52, X65, X70, X100), and three were materials used to produce NIST Charpy verification specimens at low-, high-, and super-high-energy levels (two quenched and tempered AISI 4340 steels with different heat treatments, and a 18 % Ni maraging steel designated T200). The chemical composition of the seven steels is provided in Table . Additional information can be found in [2,3].

The four investigated line pipe steels represent a variety of different material behaviors and manufacturing processes. X52 was produced in the early 60s and put in service in 1964 in a natural gas pipeline, which was extracted from the ground after 40 years of operation. X65 and X70 represent more modern and very high ductility and toughness materials. X100, although of recent production, exhibits a lower ratio between ductility and mechanical strength [2]. Three of the four line pipe steels (X52 is the exception) are microalloyed with Nb and Ti, which results in grain refinement during steel processing. The remaining three steels (4340 and T200) correspond to three

batches of NIST Charpy verification specimens: LL141 (low energy), HH143 (high energy), and SH38 (super-high energy) [3].

The type of Charpy specimens tested for each of the seven steels is summarized in Table .

Charpy tests on CVN and SCVN specimens were performed on an instrumented pendulum with capacity of 953.6 J and impact speed of 5.5 m/s. When testing SCVN specimens, shims were placed on the machine supports in order to maintain the position of the center of strike. MCVN specimens were tested by means of an instrumented small-scale pendulum with capacity of 50.8 J and impact speed of 3.5 m/s.

The instrumented striker used for CVN and SCVN specimens had a striking edge with 8 mm radius, compliant with ASTM E23 [4]. The instrumented strikers used for MCVN tests had a radius of the striking edge of 3.86 mm and 2 mm for RHS and KLST specimens, respectively.

For tests above room temperature, specimens were heated by means of an electric plate. Below room temperature, specimens were cooled in an ethyl alcohol bath down to -90 °C; for lower temperatures, liquid nitrogen (LN_2) was used. To mitigate the temperature gradient for MCVN specimens after removal from the cooling medium, the anvils and supports of the machine were maintained at low temperature (between -30 °C and -60 °C).

Additional details on the experimental setup can be found in [2,3].

DATA ANALYSIS

For each impact test performed, absorbed energy (*KV*), lateral expansion (*LE*), and shear fracture appearance (*SFA*) were measured and reported. Each parameter was then fitted as a function of test temperature by means of the commonly used hyperbolic tangent model [5], expressed as:

$$Y = A + B\,tanh\left(\frac{T - DBTT}{C}\right) \tag{1}$$

where *T* is test temperature (°C), *Y* is *KV* (J), *LE* (mm), or *SFA* (%), and *A*, *B*, *DBTT*, and *C* are fitting coefficients that are calculated by the least-square method. Note that:

- (*A* + *B*) corresponds to the upper shelf value, or the asymptotic level approached by *Y* when $T \to +\infty$;
- (*A* – *B*) corresponds to the lower shelf value, or the asymptotic level approached by *Y* when $T \to -\infty$;
- 2*C*, in °C, is the width of the transition region (portion of the curve between lower and upper shelf);
- *DBTT* (Ductile-to-Brittle Transition Temperature), in °C, is the temperature at the midpoint between lower and upper shelf;
- *B*/*C* is the slope of the fitted curve at *T* = *DBTT*.

The following constraints were applied when fitting results:

(a) the upper shelf for *KV* and *LE* (*A*+*B*) was set as the average for all specimens with *SFA* ≥ 95 %[4];

[4] This upper shelf definition is given in ASTM E185 (*Standard Practice for Design of Surveillance Programs for Light-Water Moderated Nuclear Power Reactor Vessels*).

(b) for *SFA*, *A* = *B* = 50 %, so that *DBTT* (designated as $FATT_{50}$[5]) always corresponds to *SFA* = 50 %.

Between 9 and 13 specimens were tested to obtain Charpy transition curves. Test temperatures were chosen in order to achieve a clear definition of lower shelf, upper shelf, and transition region.

As far as instrumented test results are concerned, the following parameters were determined and reported:

- force at general yield (F_{gy}), maximum force (F_m), force at the initiation of brittle fracture (F_{bf}), force at crack arrest (F_a);
- corresponding absorbed energy[6] values (W_{gy}, W_m, W_{bf}, W_a), as well as total absorbed energy (W_t).

The analysis of the instrumented force/displacement test records was performed in accordance with ASTM E2298 [6] and ISO 14556:2000 [7]. The results of these analyses are not reported here, and will be the subject of a future publication.

PRELIMINARY EXAMINATION OF TEST RESULTS

Detailed test results of the instrumented Charpy tests performed are not reported here for the sake of conciseness, and can be found in [2,3]. We report however in Table the values of $DBTT_{KV}$, $DBTT_{LE}$, $FATT_{50}$, and *USE* (Upper Shelf Energy) for all the materials and specimens tested.

[5] *FATT* stands for Fracture Appearance Transition Temperature.
[6] For an instrumented impact test, absorbed energy *W* is calculated from the force/displacement curve, whereas *KV* is provided by the machine encoder.

The following remarks concerning some of the transition curves of the NIST reference materials (LL141, HH143, SH38) will be provided below, since they are relevant to the analyses detailed hereinafter.

1. For LL141, both *KV* and *LE* transition curves do not show a plateau and appear to increase beyond the maximum test temperature (300 °C), see Fig. 1. Hence, values of *DBTT* and *USE* are associated with significant uncertainty and should be treated with caution.
2. LL141, HH143, and SH38 exhibit relatively high lower shelf levels for all measured quantities. In the case of SH38, *SFA* values above 25 % were measured down to the lowest test temperature (-198 °C), thus increasing the uncertainty of $FATT_{50}$ (Fig. 2).

Particularly for LL141, the uncertainties in *DBTT* values for the different specimen types produce results which deviate from the typical pattern of transition temperatures decreasing with specimen size, which has been reported by many investigators [8-16]. See for example the comparison between $DBTT_{KV}$ values for X52 and LL141 in Fig. 3.

Another indication of the significant uncertainties associated with some of the transition temperatures for LL141 and SH38 is illustrated in Fig. 4, which compares $DBTT_{KV}$, $DBTT_{LE}$, and $FATT_{50}$ values for the three NIST reference steels.

Under normal circumstances, the three definitions of transition temperature are expected to agree within ± 25 °C. As seen in Fig. 4, this is often not the case for LL141 and to a lesser degree for SH38. We therefore decided to exclude from further analyses all material/specimen combinations corresponding to points falling outside the ± 25 °C

tolerance bounds in Fig. 4. Even though arbitrary, this decision appeared to us a reasonable approach to deal with excessive scatter in experimental data.

CORRELATIONS BETWEEN CHARPY SPECIMEN TYPES

Ductile-to-Brittle Transition Temperatures

Figure 5 shows the average values calculated for the transition temperature shifts ($DBTT_{CVN} - DBTT_{SCVN/MCVN}$) for each non-standard specimen type investigated, considering *KV*, *LE*, and *SFA*. The data in Fig. 5 confirm that the magnitude of the shift decreases with decreasing specimen cross section, as previously reported by many authors [8-16].

Several investigators have proposed empirical correlations between transition temperature shifts and various dimensional parameters for sub-size or miniaturized Charpy specimens, such as thickness, cross sectional area or normalized fracture volume.

Both Towers [13] and Wallin [15] have correlated temperature shifts ΔT with specimen thickness *B*, respectively suggesting the following correlations:

$$\Delta T = 0.7(10 - B)^2 \tag{2}$$

$$\Delta T = -51.4 \cdot ln\left[2\left(\frac{B}{10}\right)^{0.25} - 1\right] \tag{3}$$

In eq. (2), transition temperature is defined as the temperature corresponding to an energy density of 0.25 J/mm^2 (20 J for CVN specimens). Eq. (3), on the other hand, was obtained by fitting temperature shifts based on transition temperatures calculated

for energy densities in the range 0.25 J/mm^2 to 0.5 J/mm^2 (20 J to 40 J for CVN specimens).

Various transition temperature shifts ($\Delta DBTT_{KV}$, $\Delta DBTT_{LE}$, $\Delta FATT_{KV}$, $\Delta T_{0.25J/mm2}$, $\Delta T_{0.5J/mm2}$) are plotted in Fig. 6 as a function of specimen thickness for all tests performed. The figure compares experimental data points with eqs. (2) and (3). Despite a significant amount of scatter, our test results generally appear to follow the trends of eqs. (2) and (3). It is interesting to note that, although for KLST and RHS specimens thickness is just one of the reduced dimensions, their results seem to follow the same trend as SCVN specimens.

The scatter is considerably reduced if only transition temperatures based on energy density ($T_{0.25J/mm2}$, $T_{0.5J/mm2}$) are considered, see Fig. 7. The one data point which appears to be a clear outlier corresponds to $\Delta T_{0.25J/mm2}$ for RHS specimens of LL141. Note also that in several instances $T_{0.25J/mm2}$ is undefined because the lower shelf of the transition curve corresponds to an energy density higher than 0.25 J/mm^2 (HH-143 – 3/4-size, 1/2-size, 1/4-size; SH38 – all specimen types). Similarly, in a few cases $T_{0.5J/mm2}$ is undefined because the upper shelf of the transition curves corresponds to an energy density lower than 0.5 J/mm^2 (LL141 – all specimen types; SH-38 – 1/4-size; X52 – KLST specimens).

In order to screen potential outliers, we decided to remove from the database any material/specimen combination for which $\Delta DBTT_{KV}$ differed by more than ± 25 °C from $\Delta DBTT_{LE}$ or $\Delta FATT_{50}$, see Fig. 8. The same screening criterion was applied to the comparison between $\Delta T_{0.25J/mm2}$ and $\Delta T_{0.5J/mm2}$, see Fig. 9. Note that the single outlier in Fig. 9 corresponds to the same outlier data point already outlined in Fig. 7.

The remaining database of temperature shifts was fitted by means of a logarithmic relationship, following Wallin's example [15], and the results are illustrated in Fig. 10.

The regression function obtained in Fig. 10:

$$\Delta T = 30 \cdot ln(B) - 66.2 \tag{4}$$

is extremely close to both eqs. (2) and (3), but particularly to Towers' empirical model [13]. Eq. (4) yields a Mean Square Error MSE = 237 (°C)^2 and a Mean Residual MR = 0.07 °C.

We also correlated our "filtered" database with the SCVN/MCVN ligament cross section s (in mm^2), in consideration of the fact that MCVN specimens have both cross section dimensions (thickness and width) reduced, and not just the thickness. A reasonably linear relationship is apparent in Fig. 11:

$$\Delta T = 0.409 \cdot s - 32.71 \tag{5}$$

with the imposed constraint that ΔT = 0 for s = 80 mm^2 (CVN specimen). Eq. (5) yields a Mean Square Error MSE = 253 (°C)^2 and a Mean Residual MR = 0.47 °C. These statistics are marginally worse than those previously obtained for eq. (4).

Absorbed energies for fully ductile specimens

First and foremost, it is necessary to emphasize that any correlation between absorbed energies for different Charpy specimen types is only valid provided both specimens are in the fully ductile behavior regime (upper shelf).

The first author to propose an analytical correlation between energies absorbed by full-size and sub-size Charpy specimens was Curll in 1959 [11]:

$$E_{SCVN} = \left[K\left(1 - \frac{d}{D}\right) + E_{CVN}\frac{d}{D} \right] \frac{s}{S} \tag{6}$$

where:

$E = \frac{KV}{S}$, or energy density (J/mm^2),

K = energy of rupture (29.3 J for ductile steels),

d, D = ligament size for SCVN and CVN respectively, and

s, S = cross sectional area for SCVN and CVN respectively.

Note that $d = D$ for SCVN specimens and therefore eq. (6) reduces to:

$$E_{SCVN} = E_{CVN}\frac{s}{S} \tag{7}$$

i.e., energy densities are proportional to cross sectional areas.

For each investigated material, we calculated the energy density at three or four temperatures where all tested specimen types exhibited fully ductile behavior. The results obtained are plotted in Fig. 12, where data for each SCVN/MCVN specimen type are fitted with straight lines passing through the origin (*i.e.,* $E_{SCVN/MCVN} = 0$ when $E_{CVN} = 0$). It is apparent that the tougher the material, the higher is the energy density for SCVN/MCVN specimens with respect to CVN specimens. Moreover, smaller specimens tend to provide higher energy densities.

The energy density ratio ($E_{CVN}/E_{SCVN/MCVN}$) for the investigated specimen types, taken as the slope of the linear regressions shown in Fig. 12, is plotted and fitted in Fig. 13 as a function of cross sectional area. In the figure, data are compared to eq. (7) from Curll, which in principle only applies to SCVN specimens. The relationship obtained is:

$$\frac{E_{SCVN/MCVN}}{E_{CVN}} = 0.293 ln(s) - 0.3821 \quad (8)$$

If only SCVN are fitted, the equation of the linear regression is:

$$\frac{E_{SCVN}}{E_{CVN}} = 0.0063s + 0.431 \quad (9)$$

In both cases, energy densities for non-standard specimens are significantly higher than given by Curll in [11].

Upper Shelf Energy (USE) Values

The most commonly used approach for correlating *USE* values between Charpy specimens of different geometries involves the use of a normalization factor, *NF*, which can be empirically derived from experimental data or calculated as the ratio between specific geometric parameters:

$$USE_{CVN} = NF \cdot USE_{SCVN/MCVN} \quad (10)$$

Published values of *NF* include:

- NF_1 = ratio of fracture areas, expressed as Bd, where d is the ligament size [17,18];
- NF_2 = ratio of nominal fracture volumes, expressed as $(Bd)^{3/2}$ [17,18];
- NF_3 = ratio of nominal fracture volumes, expressed as Bd^2 [19,20];
- NF_4 = ratio of Bd^2/AK_t (with A = span, or distance between the anvils, and K_t = elastic stress concentration factor, which depends on ligament size and notch root radius) [21];

- NF_5 = ratio of $(Bd)^{3/2}/QK_t$ (with Q = plastic stress concentration factor, given by $Q = 1 + (\pi - \theta)/2$, where θ is the notch angle in radians) [22].

Additionally, empirical normalization factors were published by Sokolov and Alexander for 4 types of miniaturized Charpy specimens [23] (NF_6) and by Lucon *et al.* for KLST specimens [24] (NF_7).

The empirical normalization factors NF_8 calculated in this study by fitting the experimental *USE* values given in Table 3 are provided in Table 4, which compares them to the geometrical and empirical factors listed above.

Geometrical and empirical factors are plotted in Fig. 14 as a function of cross sectional area. Our results are in good agreement with both NF_2 (ratio of nominal fracture volumes $(Bd)^{3/2}$) and NF_3 (ratio of nominal fracture volumes Bd^2). Exponentially fitting our test results yields:

$$\frac{USE_{CVN}}{USE_{SCVN\,/\,MCVN}} = 899.14 \cdot s^{-1.599} \tag{11}$$

with coefficient of determination $R^2 = 0.98$.

In Fig. 14 the largest discrepancies are observed for KLST specimens. For this MCVN geometry, the results we obtained on line pipe steels were also compared in Fig. 15 to the following exponential fit, which was obtained in [24] from a number of reactor pressure vessel (RPV) ferritic steels:

$$USE_{CVN} = 29.454 \cdot e^{0.2378 \cdot USE_{KLST}} \tag{12}$$

The agreement between our results and eq. (12) is reasonable, although USE_{CVN} is underestimated for X65 and X70, which have significantly higher toughness and strength than typical RPV steels.

NIST VERIFICATION SPECIMENS FOR SMALL-SCALE PENDULUM MACHINES

Reference full-size Charpy specimens used for the indirect verification of impact machines, produced by National Metrology Institutes such as NIST in the US and IRMM (Institute for Reference Materials and Measurements) in the European Union, cannot be used to verify small-scale impact machines, having capacity between 15 J and 50 J.

NIST in Boulder Colorado has recently qualified miniaturized KLST specimens, which can be used to verify small-scale machines at three energy levels: low energy (1.59 J), high energy (5.65 J), and super-high energy (10.03 J). The same reference specimens can also be used to verify the force scale if the striker is instrumented: certified maximum force values are 2.43 kN, 1.78 kN, and 1.79 kN at the three energy levels respectively. KLST verification specimens are tested at room temperature (21 °C ± 3 °C), and are available in sets of three samples.

Certified reference values for both maximum force and absorbed energy were established by means of an interlaboratory exercise (Round-Robin), which was coordinated by NIST and involved nine qualified international laboratories, mostly European. The Round-Robin results were analyzed by NIST in accordance with both ISO 5725-2 [25] and ASTM E691 [26], as well as standard procedures of the Charpy Verification Program at NIST [27].

Full details for this activity are available elsewhere [28,29].

CONCLUSIONS

The study presented here was aimed at correlating impact test results from Charpy specimens of different configurations (full-size, sub-size, and miniaturized). The materials investigated included four line pipe steels of varying toughness and strength, as well as three steels used by NIST for the fabrication of Charpy verification specimens. Four sub-size specimen types (3/4-size, 2/3-size, 1/2-size, and 1/4-size) and two miniaturized specimen types were considered (RHS and KLST). The main conclusions which emerged from the study are summarized below.

1. As generally reported in the literature, ductile-to-brittle transition temperatures (expressed in relation to different variables) were found to decrease with specimen size, mainly as a result of diminishing stress triaxiality and loss of constraint.
2. The transition temperature shift caused by size reduction can be correlated to specimen thickness for both sub-size and miniaturized specimens, even though for the latter both thickness and width are reduced with respect to full-size specimens. The empirical correlation we established is in good agreement with those proposed by Towers and Wallin. A simpler linear correlation was also obtained as a function of ligament cross section.
3. A direct correlation between Charpy energies absorbed by CVN and SCVN/MCVN specimens is only possible if the behavior is fully ductile for both specimens. In this

case, we established a logarithmic empirical correlation between the ratio of absorbed energies and the area of the MCVN/SCVN cross section.

4. As far as the correlation of Upper Shelf Energies is concerned, our test results were compared with several normalization factors ($NF = USE_{CVN}/USE_{SCVN/MCVN}$) published in the literature. A strong exponential correlation with cross sectional area was found, in close agreement with the normalization factor based on the ratio of nominal fracture volumes Bd^2.
5. In general, we found that the same relationships can be used to correlate the behavior of full-size specimens with that of both sub-size specimens (where only the thickness is reduced) and miniaturized specimens (where both thickness and width are reduced). Cross sectional area appears to be an effective independent variable for the correlations.
6. In all cases, a significant amount of data scatter was observed. As a consequence, any full-size specimen prediction based on the empirical correlations obtained is subject to considerable uncertainty. Material-specific correlations (*e.g.* for line pipe steels, for RPV steels, etc.) may provide more accurate predictions.
7. The correlations in this study were obtained after screening possible outliers by comparing various measures of transition temperatures ($DBTT_{KV}$, $DBTT_{LE}$, $FATT_{50}$, $T_{0.25J.mm2}$, $T_{0.5J/mm2}$). If any of the different measures differed by more than ± 25 °C, the material/specimen combination was excluded by subsequent analyses. This could be adopted as a reasonable “quality check” for future investigations.

REFERENCES

[1] Towers, O. L., 1986, "Testing sub-size Charpy specimens. Part 3–The adequacy of current code requirements," Metal Construction, pp. 319R-325R.
[2] Lucon, E., McCowan, C. N., and Santoyo, R. L., 2014, "Impact Characterization of Line Pipe Steels by Means of Standard, Sub-Size and Miniaturized Charpy Specimens," NIST Technical Note 1865, NIST, Boulder CO (USA).
[3] Lucon, E., McCowan, C. N., and Santoyo, R. L., 2014, "Impact Characterization of 4340 and T200 Steels by Means of Standard, Sub-Size and Miniaturized Charpy Specimens," NIST Technical Note 1858, NIST, Boulder CO (USA).
[4] ASTM E23-12c, "Standard Test Methods for Notched Bar Impact Testing of Metallic Materials," ASTM Book of Standards, Vol. 03.01, ASTM International, West Conshohocken, PA.
[5] Oldfield, W., 1975, "Curve Fitting Impact Test Data: A Statistical Procedure," ASTM Standardization News, pp. 24-29.
[6] ASTM E2298-13a, "Standard Test Method for Instrumented Impact Testing of Metallic Materials," ASTM Book of Standards, Vol. 03.01, ASTM International, West Conshohocken, PA.
[7] ISO 14556:2000, "Steel -- Charpy V-notch pendulum impact test -- Instrumented test method," International Standards Organization, Geneva, Switzerland.
[8] Zeno, R.S. and Dolby, J. L., 1953, "The Effect of Specimen Geometry on Impact Transition Temperature," Welding Research Supplement, pp. 190s-197s.
[9] Zeno, R.S., 1956, "Effect of Specimen Width on the Notched Bar Impact Properties of Quenched-and-Tempered and Normalized Steels," in "Symposium on Impact Testing," F. Tatnall, ed., ASTM STP176, ASTM, Philadelphia PA, pp. 59-69. DOI: 10.1520/STP47577S
[10] Curll, C. H. and Orner, G. M., 1958, "Correlation of Selected Subsize Charpy Bars Versus the Standard Charpy Bar," Technical Report 112/91, Watertown Arsenal Laboratories, Watertown MA.
[11] Curll, C. H., 1959, "Subsize Charpy Correlation with Standard Charpy," Technical Report 112/95, Watertown Arsenal Laboratories, Watertown MA.
[12] McNicol, R. C., 1965, "Correlation of Charpy Test Results for Standard and Nonstandard Size Specimens," Welding Research Supplement, pp. 383s-393s.
[13] Towers, O. L., 1983, "Charpy V-Notch Tests: Influences of Striker Geometry and of Specimen Thickness," Research Report 219/1983, The Welding Institute.
[14] Towers, O. L., 1986, "Testing sub-size Charpy specimens. Part 1–The influence of thickness on the ductile/brittle transition," Metal Construction, pp. 171R-176R.
[15] Wallin, K., 1994, "Methodology for selecting Charpy toughness criteria for thin high strength steels: Part 1 - determining the fracture toughness," Jernkontorets Forskning, Report from Working Group 4013/89, Espoo, Finland.
[16] TWI Knowledge Summary, 2011, "Sub-size Charpy Specimens," The Engineering Institution for Welding and Joining Professionals, TWI Ltd, Cambridge, UK.

[17] Corwin, W. R., Klueh, R. L., and Vitek, J. M., 1984, "Effect of Specimen Size and Nickel Content on the Impact Properties of 12 Cr-1 MoVW Ferritic Steel," Journal of Nuclear Materials **122-123**, pp. 343-348. DOI: 10.1016/0022-3115(84)90622-6
[18] Corwin, W. R. and Hougland, A. M., 1986, "Effect of Specimen Size and Material Condition on the Charpy Impact Properties of 9Cr-1Mo-V-Nb Steel," in "The Use of Small-scale Specimens for Testing Irradiated Material," W. R. Corwin and G. E. Lucas, eds., ASTM STP 888, ASTM, Philadelphia, pp. 325-338.
[19] Lucas, G. E., Odette, G. R., Sheckherd, J. W., McConnell, P., and Perrin, J., 1986, "Subsized Bend and Charpy V Notch Specimens for Irradiated Testing," in "The Use of Small-scale Specimens for Testing Irradiated Material," W. R. Corwin and G. E. Lucas, eds., ASTM STP 888, ASTM, Philadelphia, pp. 304-324.
[20] Lucas, G. E., Odette, G. R., Sheckherd, J. W., and Krishnadev, M. R., 1986, "Recent Progress in Subsized Charpy Impact Specimen Testing for Fusion Reactor Materials Development," Fusion Technology **10**, pp. 728-733.
[21] Louden, B. S., Kumar, A. S., Garner, F. A., Hamilton, M. L., and Hu, W. L., 1988, "The Influence of Specimen Size on Charpy Impact Testing of Unirradiated HT-9," Journal of Nuclear Materials **155-157**, pp. 662-667. DOI: 10.1016/0022-3115(88)90391-1
[22] Kayano, H., Kurishita, H., Kimura, A., Narui, M., Yamazaki, M., and Suzuki, Y., 1991, "Charpy Impact Testing Using Miniature Specimens and Its Application to the Study of Irradiation Behavior of Low-Activation Ferritic Steels," Journal of Nuclear Materials **179-181**, pp. 425-488. DOI: 10.1016/0022-3115(91)90115-N
[23] Sokolov, M. A. and Alexander, D. J., 1997, "An Improved Correlation Procedure for Subsize and Full-Size Charpy Impact Specimen Data," NUREG/CR-6379, ORNL-6888, Oak Ridge National Laboratory, Oak Ridge TN.
[24] Lucon, E., Chaouadi, R., Fabry, A., Puzzolante, J.-L., and van Walle, E., 2000, "Characterizing Material Properties by the Use of Full-Size and Subsize Charpy Tests: An Overview of Different Correlation Procedures," in "Pendulum Impact Testing: A Century of Progress," T. A. Siewert and M. P. Manahan, eds., ASTM STP 1380, ASTM International, West Conshohocken, PA, pp.146-163.
[25] ISO 5725-2:1994, "Accuracy (trueness and precision) of measurement methods and results -- Part 2: Basic method for the determination of repeatability and reproducibility of a standard measurement method," International Standards Organization, Geneva, Switzerland.
[26] ASTM E691-14, "Standard Practice for Conducting an Interlaboratory Study to Determine the Precision of a Test Method," ASTM Book of Standards Vol. 14.02, ASTM International, West Conshohocken, PA.

[27] McCowan, C. N., Siewert, T. A., and Vigliotti, D. P., 2003, “The NIST Charpy V-notch Verification Program: Overview and Operating Procedures,” in “Charpy Verification Program: Reports Covering 1989-2002,” Technical Note 1500-9, NIST Boulder CO, pp. 3-42.
[28] Lucon, E., McCowan, C. N., Santoyo, R. L., and Splett, J. D., 2013, “Certification Report for SRM 2216, 2218, 2219: KLST (Miniaturized) Charpy V-Notch Impact Specimens,” Special Publication 260-180, NIST, Boulder CO.
[29] Lucon, E., McCowan, C. N., Santoyo, R. L., and Splett, J. D., 2015, “Certified KLST Miniaturized Charpy Specimens for the Indirect Verification of Small-Scale Impact Machines,” in “Small Specimen Test Techniques: 6th Volume,” M. A. Sokolov and E. Lucon, eds., ASTM STP 1576, ASTM International, West Conshohocken PA, pp. 1–20.

Figure Captions List

Fig. 1 *KV* transition curve for LL141, CVN specimens

Fig. 2 *SFA* transition curve for SH38, CVN specimens

Fig. 3 $DBTT_{KV}$ values calculated for X52 and LL141

Fig. 4 Comparison between ductile-to-brittle transition temperatures calculated for LL141, HH143, and SH38

Fig. 5 Transition temperature shifts between CVN and SCVN/MCVN specimens, as a function of specimen cross section

Fig. 6 Calculated transition temperature shifts as a function of specimen thickness, and comparison with eq. (2) and eq. (3)

Fig. 7 $\Delta T_{0.25J/mm2}$ and $\Delta T_{0.5J/mm2}$ vs. specimen thickness, and comparison with eq. (2) and eq. (3)

Fig. 8 Comparison between $\Delta DBTT_{KV}$, $\Delta DBTT_{LE}$ and $\Delta FATT_{50}$

Fig. 9 Comparison between $\Delta T_{0.25J/mm2}$ and $\Delta T_{0.5J/mm2}$

Fig. 10 "Filtered" NIST database of transition temperature shifts, and comparison with eqs. (2) and (3)

Fig. 11 "Filtered" NIST database of transition temperature shifts as a function of ligament cross section

Fig. 12 Energy densities for CVN, SCVN, and MCVN specimens

Fig. 13 Energy density ratio as a function of SCVN/MCVN cross sectional area

Table Caption List

Table 1 - Chemical composition of the steels (wt %)

Steel	C	Mn	Si	S	P	Ni	Cr	Mo	Nb+Ti+V
X52	0.24	0.96	0.06	0.021	0.011	0.24	0.01	0.004	0.005
X65	0.05	1.42	0.28	0.003	0.011	0.05	0.04	0.01	0.051
X70	0.05	1.37	0.23	0.001	0.010	0.05	0.06	n/a	0.091
X100	0.24	0.96	0.06	0.021	0.011	0.24	0.03	0.27	0.036
4340	0.40	0.66	0.28	0.001	0.004	1.77	0.83	0.28	n/a
T200	≤0.01	≤0.01	≤0.01	≤0.01	≤0.01	18.5	n/a	3.0	n/a

Table 2 – Charpy specimens tested for each material

		SCVN				MCVN	
Steel	CVN	3/4-size	2/3-size	1/2-size	1/4-size	KLST	RHS
X52	√		√	√		√	√
X65	√		√	√		√	√
X70	√		√	√		√	√
X100	√		√	√		√	√
LL141	√	√		√	√		√
HH143	√	√		√	√		√
SH38	√	√		√	√		√

Table 3 - Transition temperatures and *USE* values obtained

Steel	Specimen type	$DBTT_{KV}$ (°C)	*USE* (J)	$DBTT_{LE}$ (°C)	$FATT_{50}$ (°C)
X52	CVN	11.7	72.6	8.4	17.8
	2/3-size	0.2	47.3	-0.8	9.0
	1/2-size	-4.3	36.0	-5.2	0.3
	KLST	-35.1	4.2	-29.6	-36.6
	RHS	-5.6	12.3	-4.8	-8.0
X65	CVN	-34.8	415.7	-75.7	-40.0
	2/3-size	-70.1	246.0	-94.6	-78.8
	1/2-size	-80.5	120.6	-102.6	-85.4
	KLST	-111.0	9.5	-110.9	-102.8
	RHS	-111.6	44.0	-114.1	-114.2
X70	CVN	-94.5	419.8	-100.3	-97.4
	2/3-size	-100.3	252.1	-104.3	-103.9
	1/2-size	-103.8	128.9	-117.2	-113.8
	KLST	-136.6	10.0	-136.2	-139.1
	RHS	-126.6	47.1	-123.5	-128.5
X100	CVN	-69.6	233.7	-74.0	-67.7
	2/3-size	-82.7	122.8	-85.2	-83.7
	1/2-size	-76.7	78.7	-78.6	-78.5
	KLST	-117.8	8.9	-115.5	-113.0
	RHS	-103.0	28.9	-103.0	-103.6
LL141	CVN	-26.1	32.0	31.0	47.1
	3/4-size	-8.5	25.8	116.5	27.2
	1/2-size	-6.5	17.1	49.7	3.6
	1/4-size	-33.2	8.2	75.3	-40.6
	RHS	-46.2	5.6	45.4	5.0
HH143	CVN	-89.8	111.4	-85.0	-102.1
	3/4-size	-93.5	79.1	-78.4	-99.4
	1/2-size	-96.2	46.2	-97.9	-107.0
	1/4-size	-125.1	18.0	-120.2	-141.6
	RHS	-115.0	15.9	-111.1	-131.4
SH38	CVN	-97.6	177.2	-88.5	-127.8
	3/4-size	-98.1	139.7	-100.8	-131.9
	1/2-size	-113.4	73.3	-113.9	-176.4
	1/4-size	-126.6	22.8	-137.1	-208.3
	RHS	-143.4	25.9	-144.5	-168.8

Table 4 - Geometrical and empirical normalization factors for SCVN and MCVN specimens

Specimen type	NF_1	NF_2	NF_3	NF_4	NF_5	NF_6	NF_7	NF_8
3/4-size	1.33	1.54	1.33	1.33	1.54	-	-	1.31
2/3-size	1.50	1.84	1.50	1.50	1.50	-	-	1.70
1/2-size	2.00	2.83	2.00	2.00	2.83	-	-	2.63
1/4-size	4.00	8.00	4.00	4.00	8.00	-	-	5.95
RHS	4.29	8.89	8.89	3.30	6.84	6.3	-	7.42
KLST	8.89	26.50	23.70	30.00	51.26	24.9	21.6	32.32

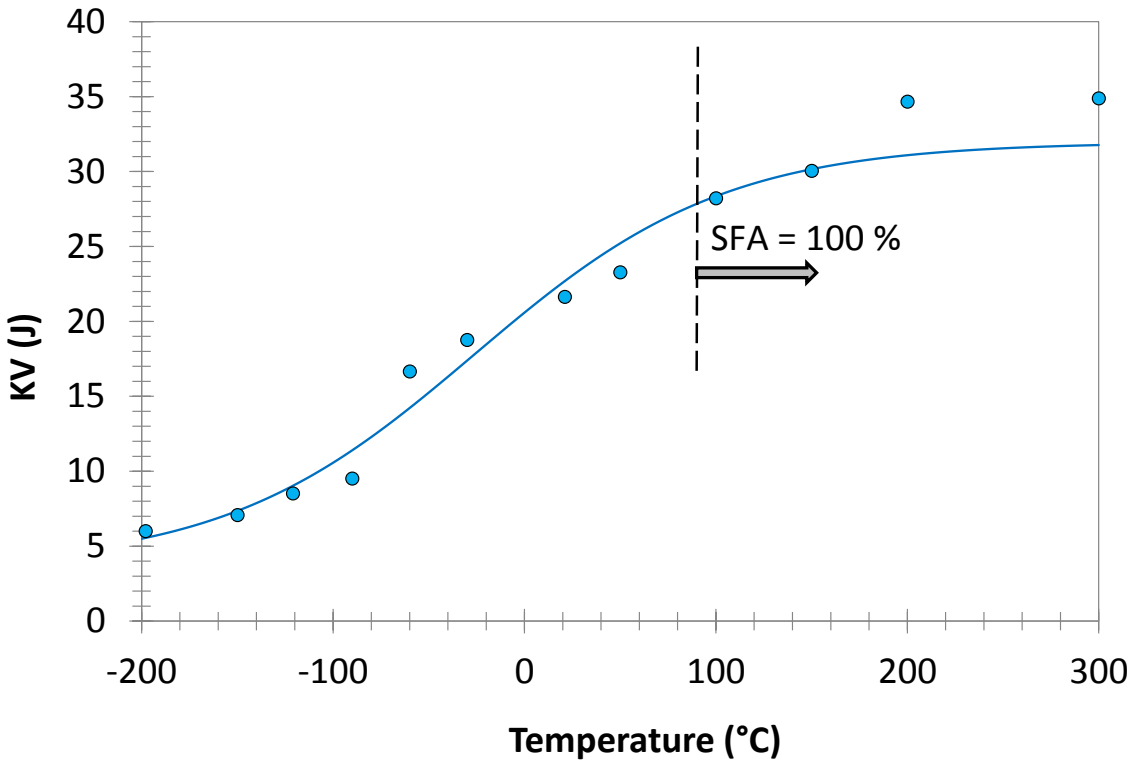

Fig. 1 - *KV* transition curve for LL141, CVN specimens

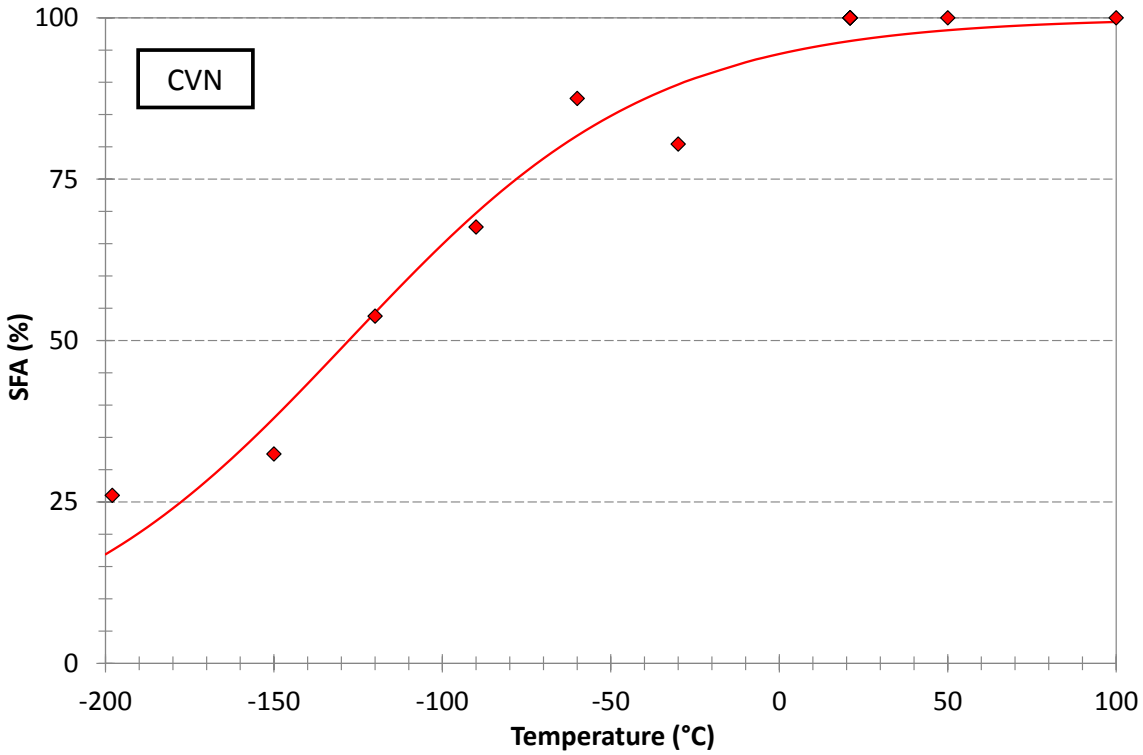

Fig. 2 - *SFA* transition curve for SH38, CVN specimens

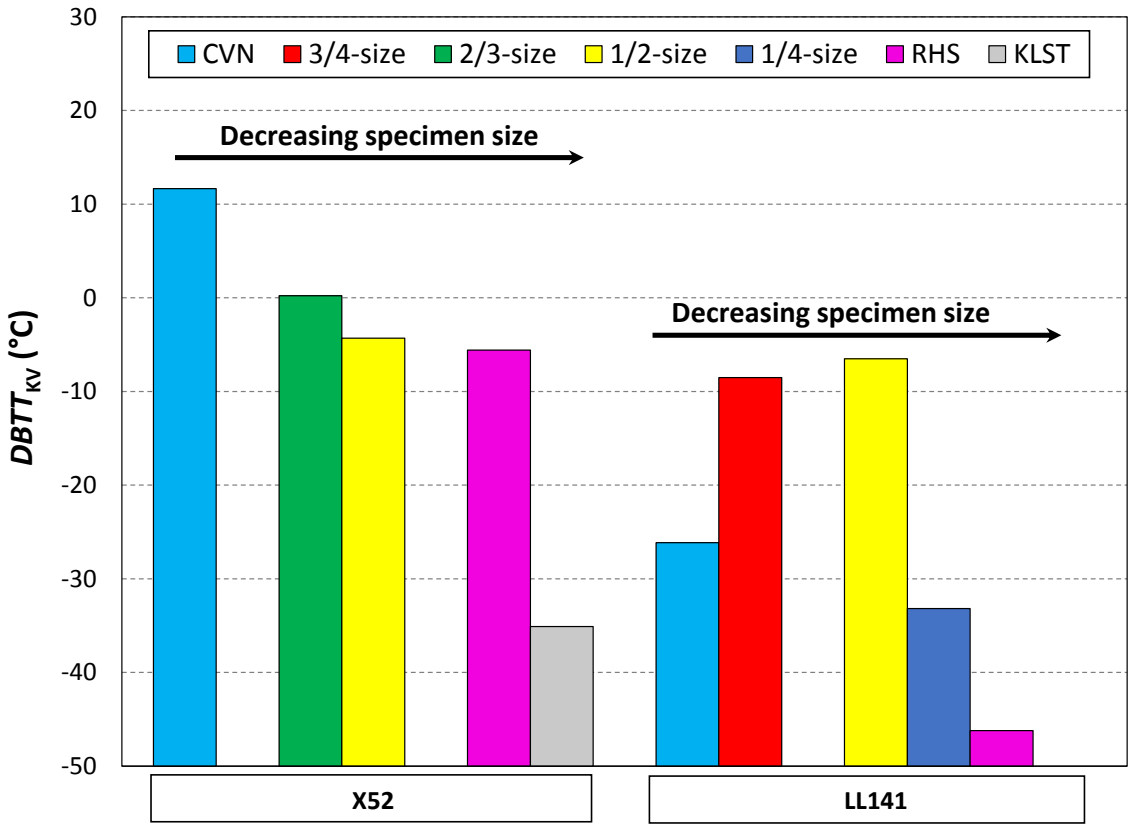

Fig. 3 – $DBTT_{KV}$ values calculated for X52 and LL141

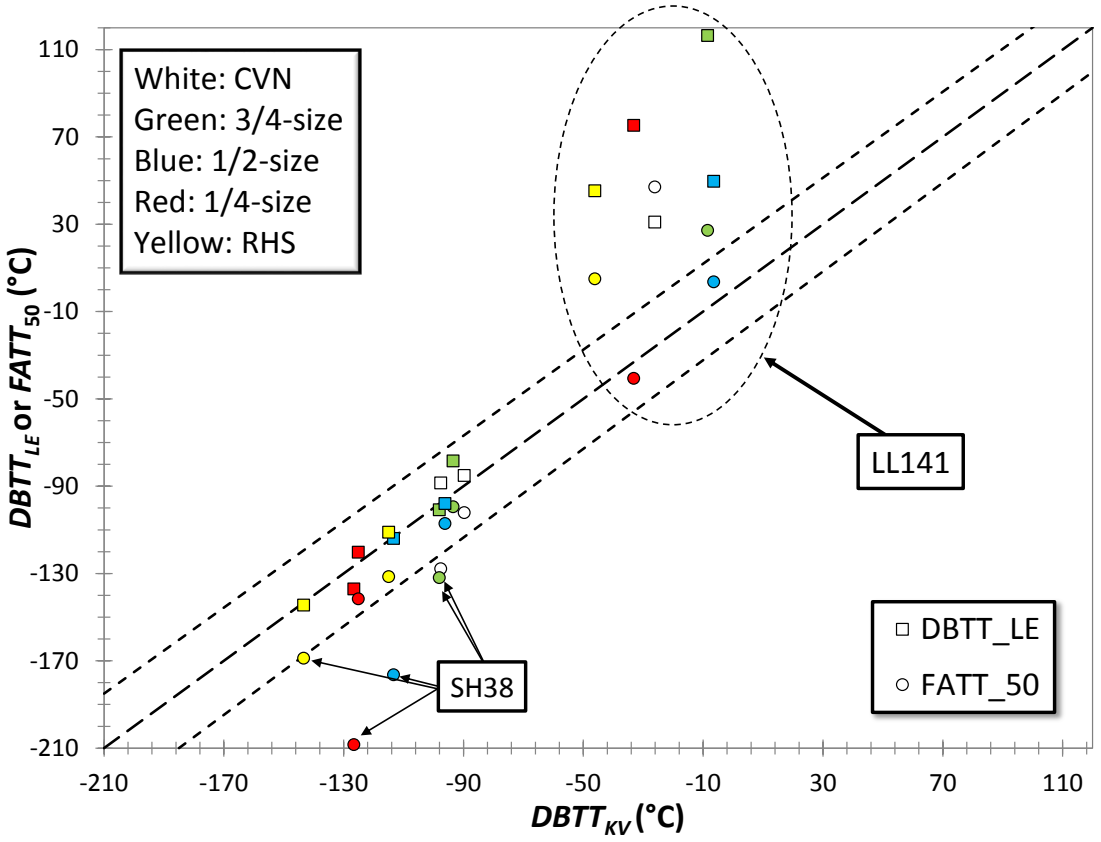

Fig. 4 – Comparison between ductile-to-brittle transition temperatures calculated for LL141, HH143, and SH38

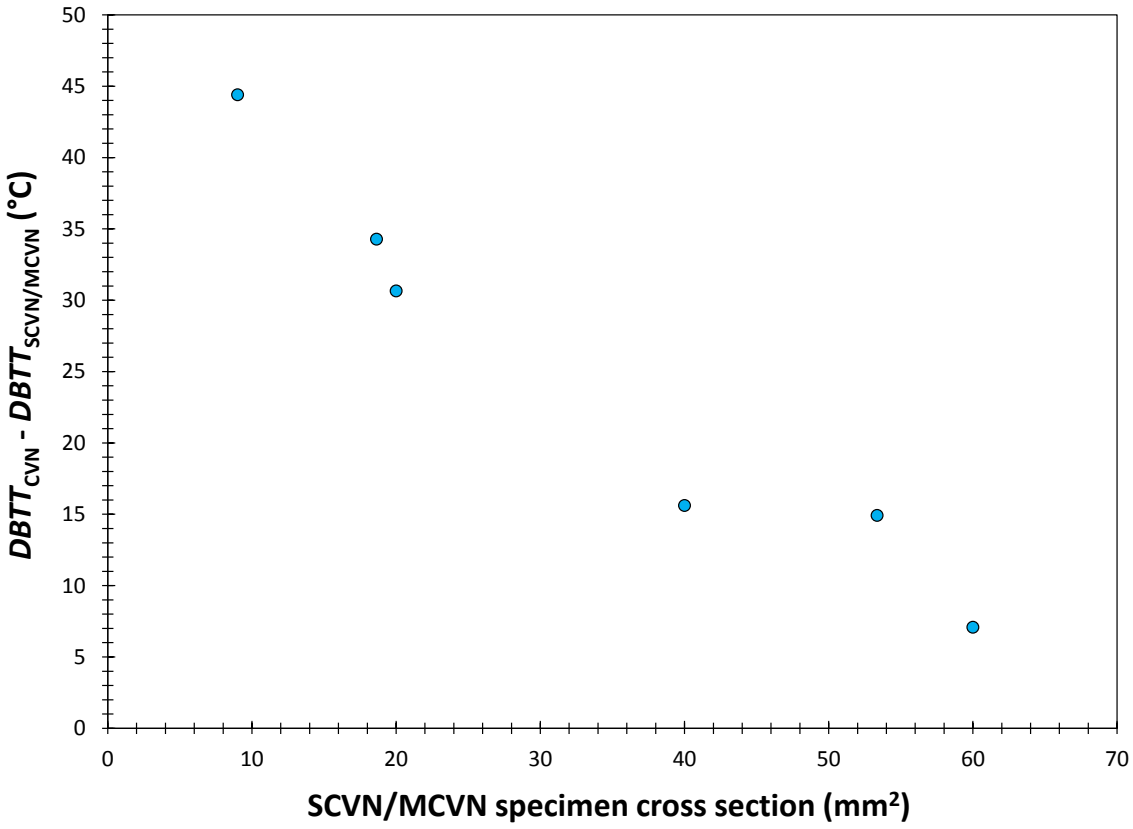

Fig. 5 – Transition temperature shifts between CVN and SCVN/MCVN specimens, as a function of specimen cross section

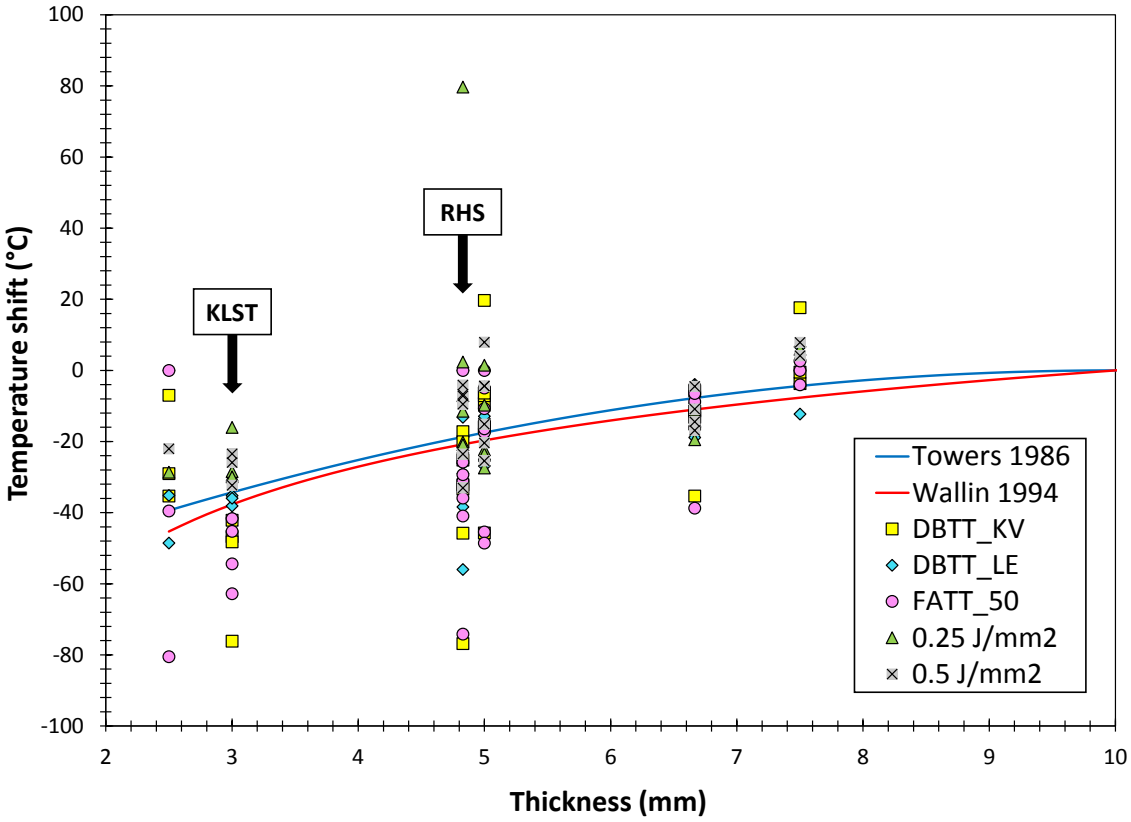

Fig. 6 – Calculated transition temperature shifts as a function of specimen thickness, and comparison with eq. (2) and eq. (3)

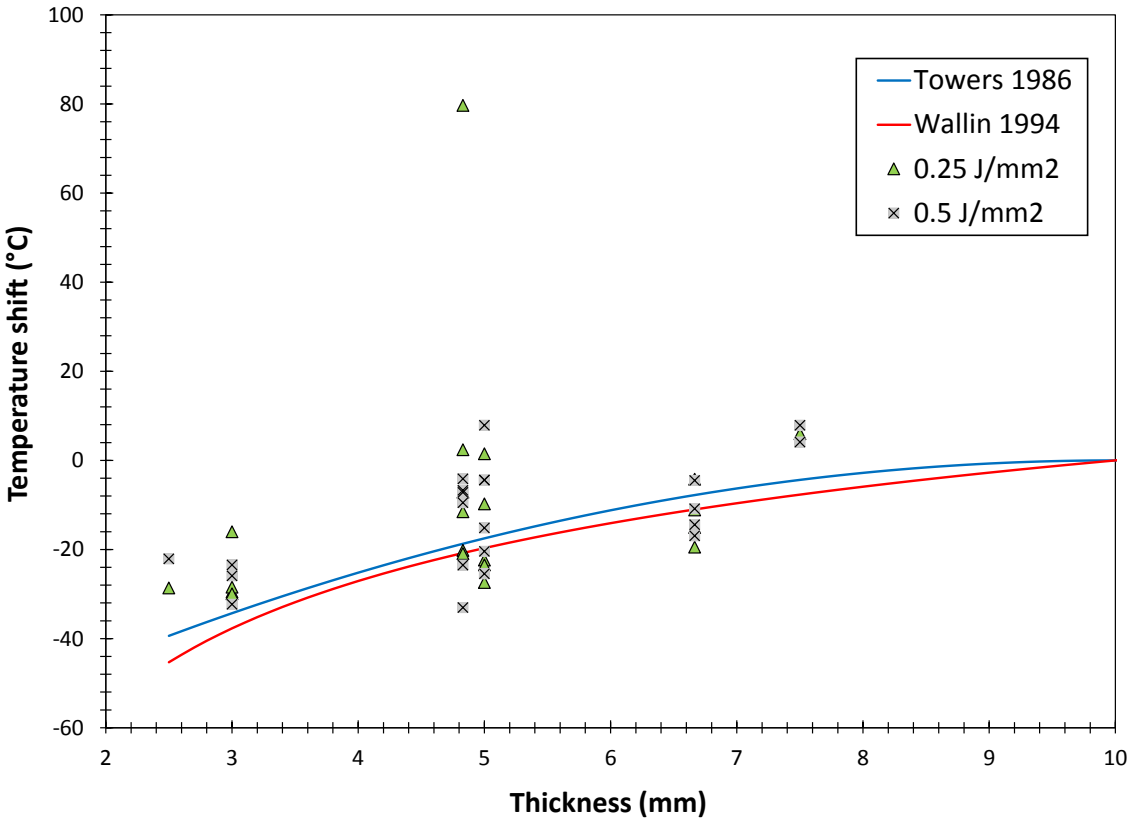

Fig. 7 – $\Delta T_{0.25J/mm2}$ and $\Delta T_{0.5J/mm2}$ vs. specimen thickness, and comparison with eq. (2) and eq. (3)

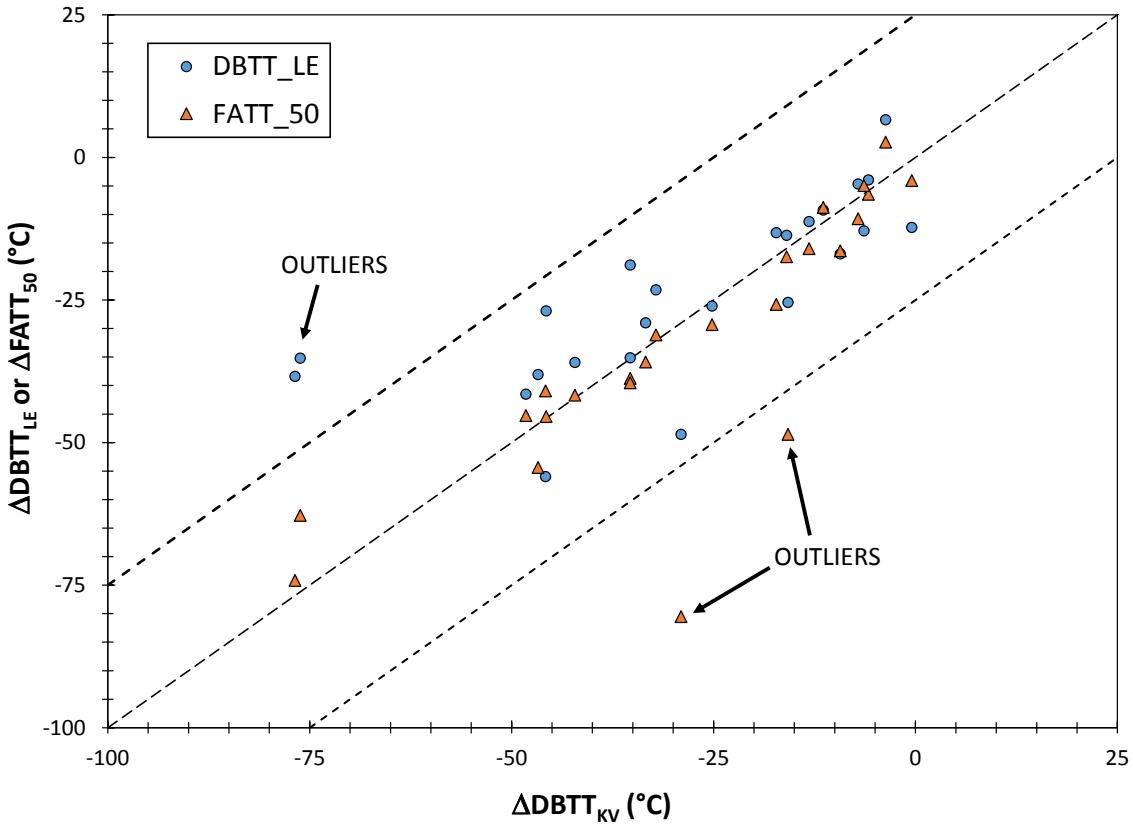

Fig. 8 – Comparison between $\Delta DBTT_{KV}$, $\Delta DBTT_{LE}$ and $\Delta FATT_{50}$.

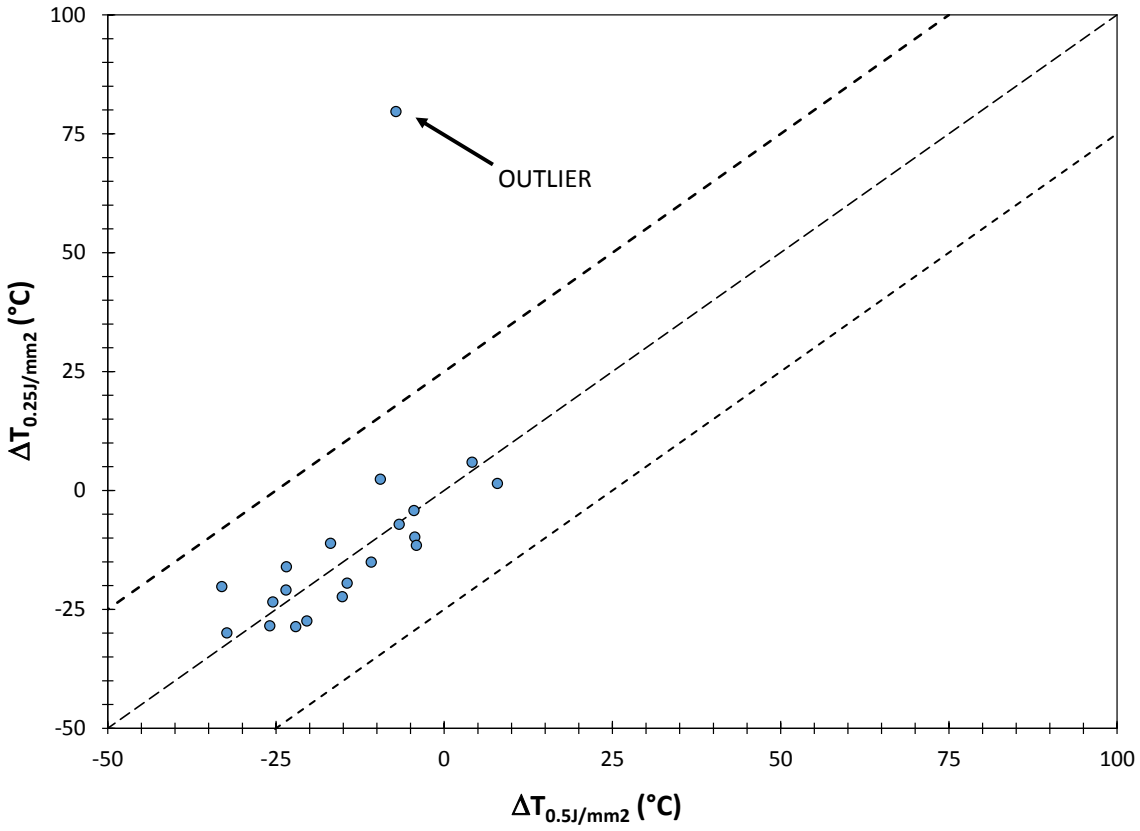

Fig. 9 – Comparison between $\Delta T_{0.25J/mm2}$ and $\Delta T_{0.5J/mm2}$

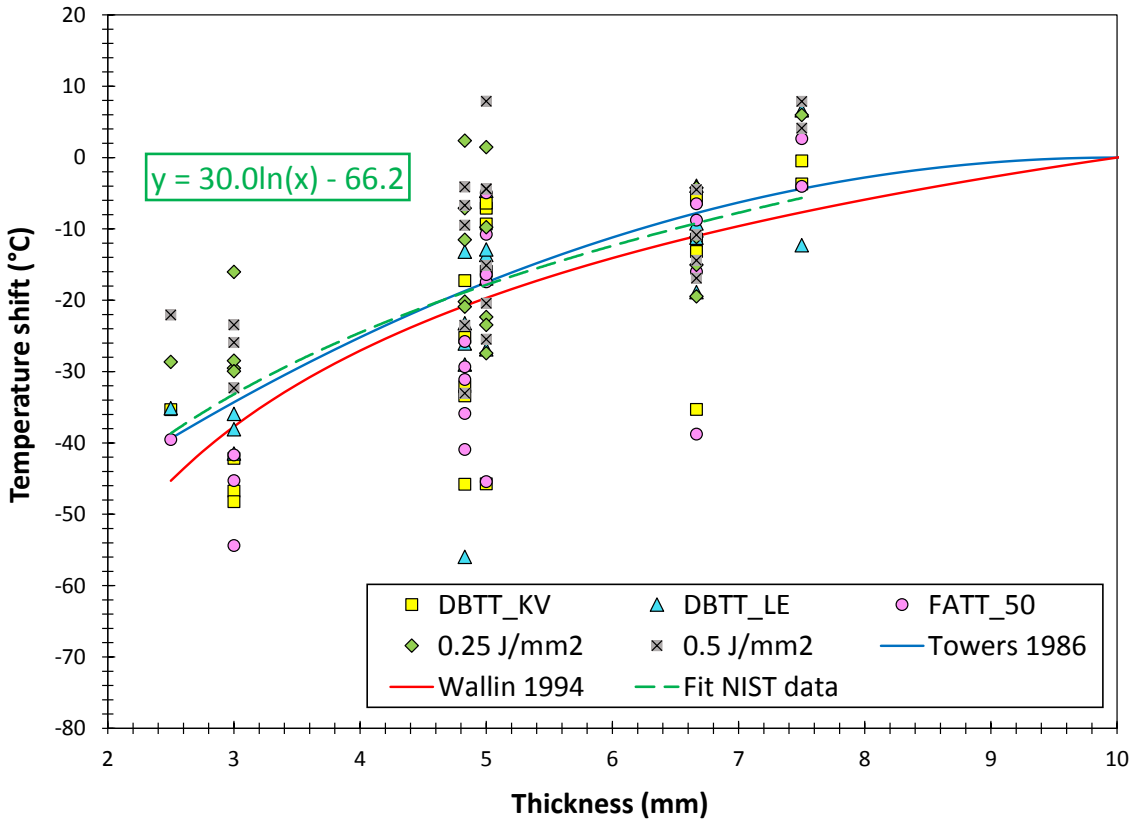

Fig. 10 – "Filtered" NIST database of transition temperature shifts, and comparison with eqs. (2) and (3)

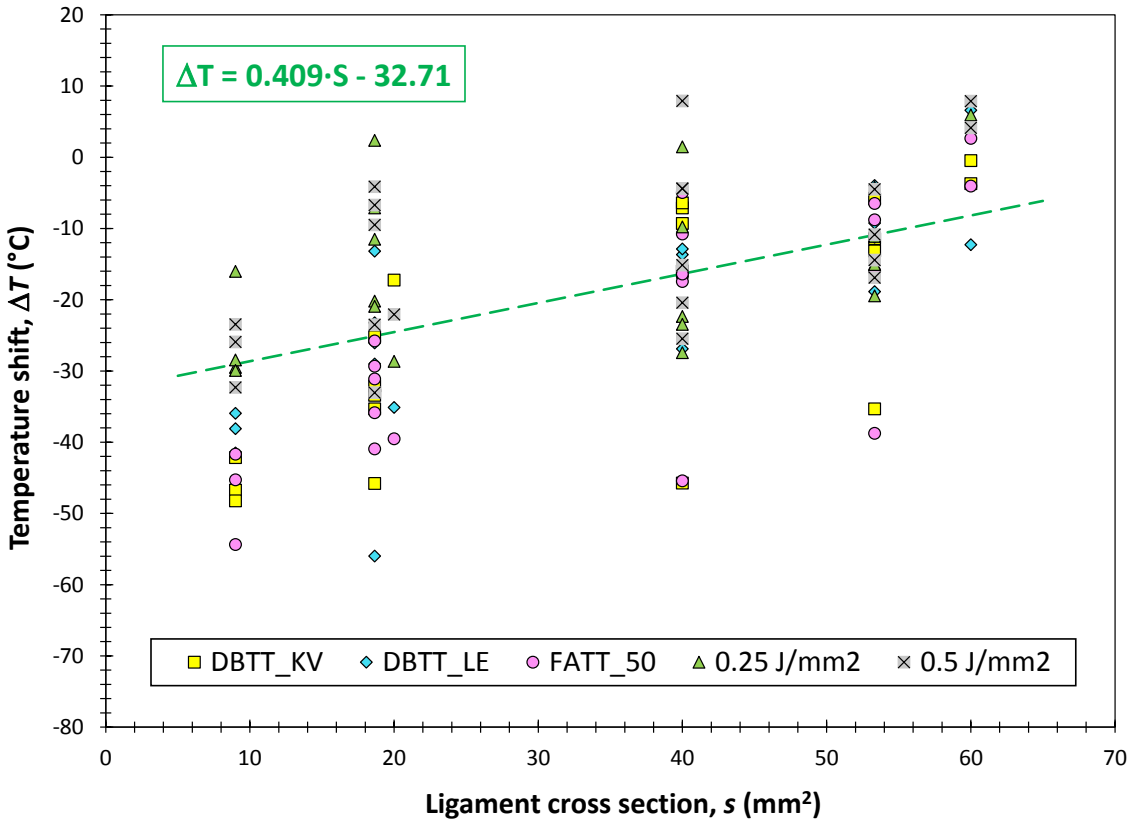

Fig. 11 – "Filtered" NIST database of transition temperature shifts as a function of ligament cross section

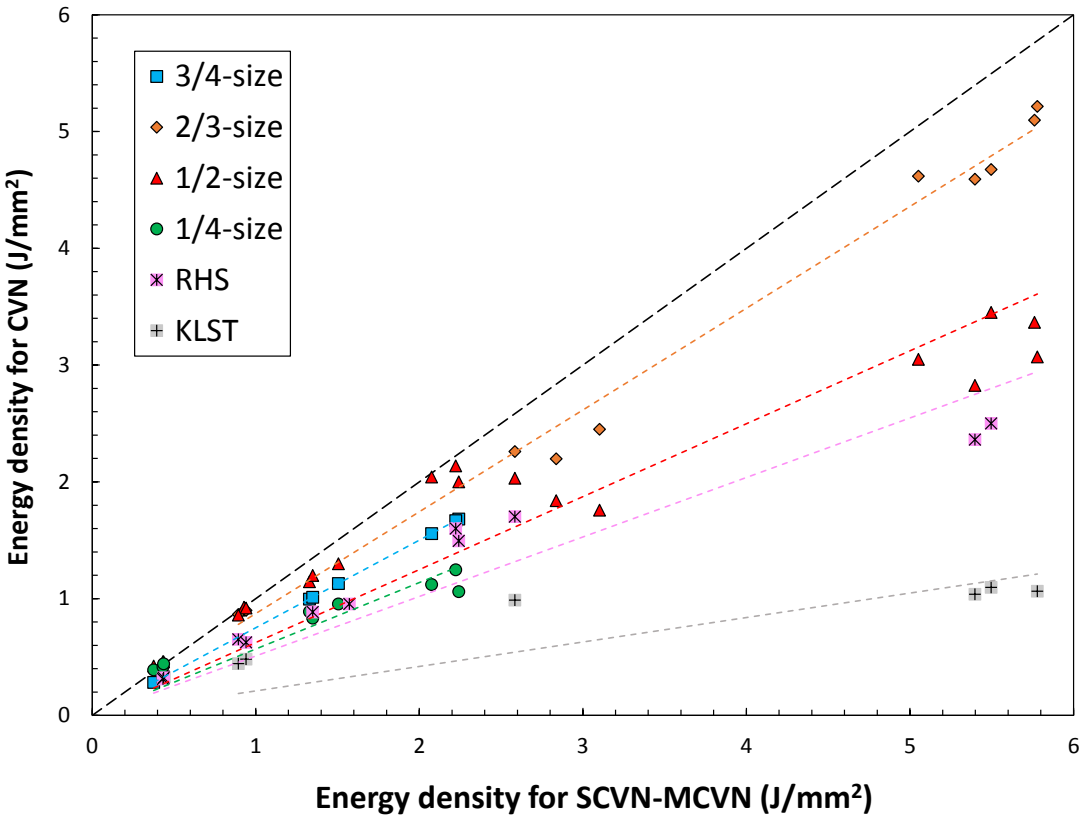

Fig. 12 – Energy densities for CVN, SCVN, and MCVN specimens

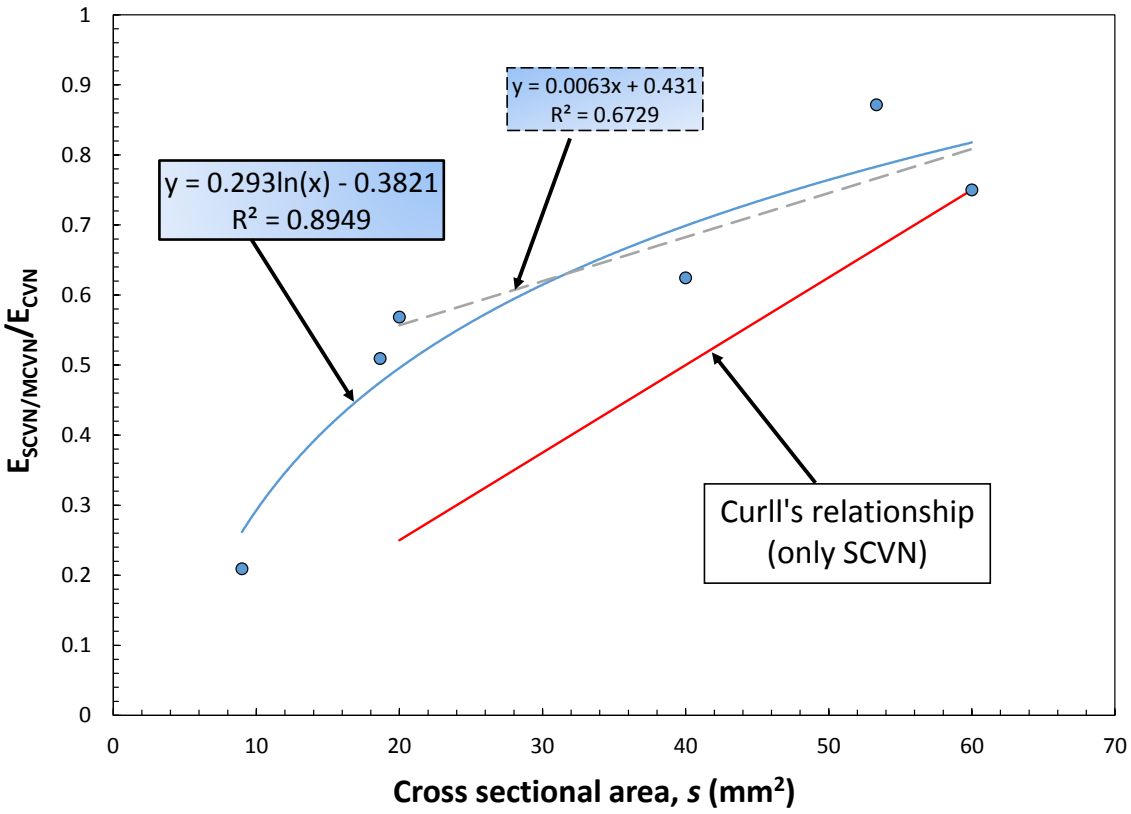

Fig. 13 – Energy density ratio as a function of SCVN/MCVN cross sectional area

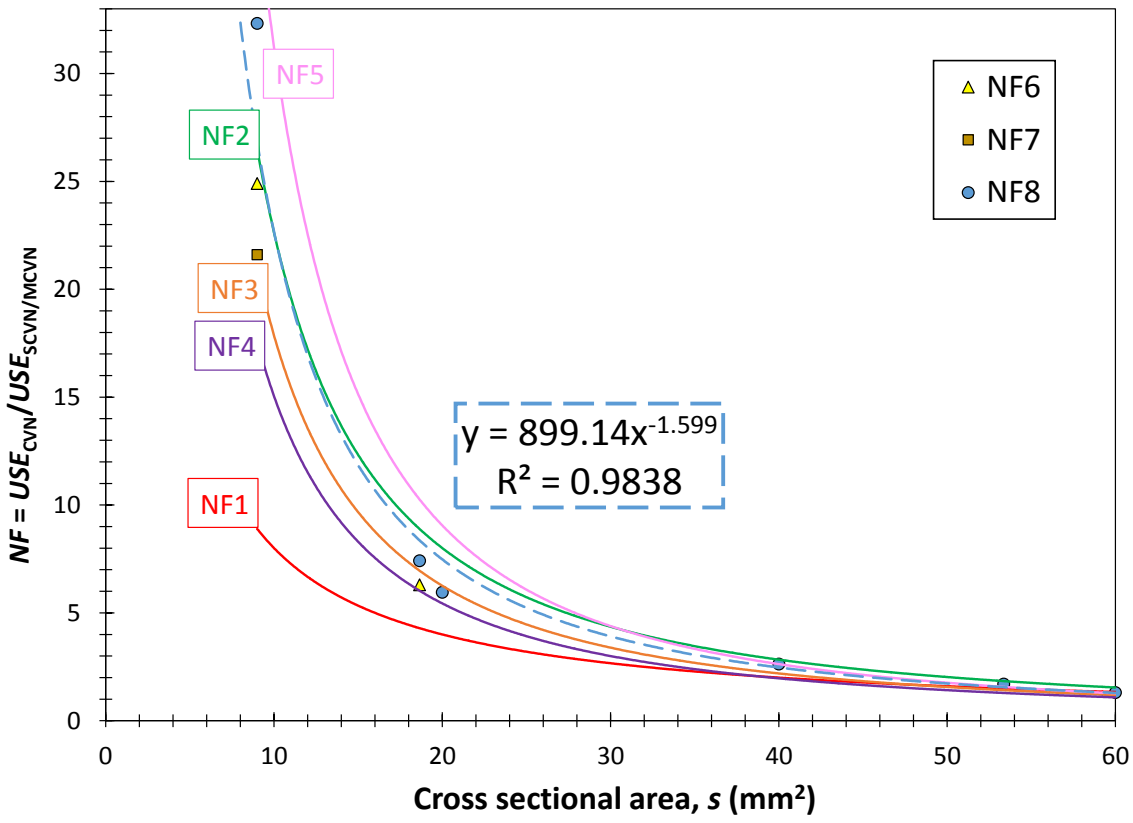

Fig. 14 - Geometrical and empirical normalization factors for SCVN and MCVN specimens

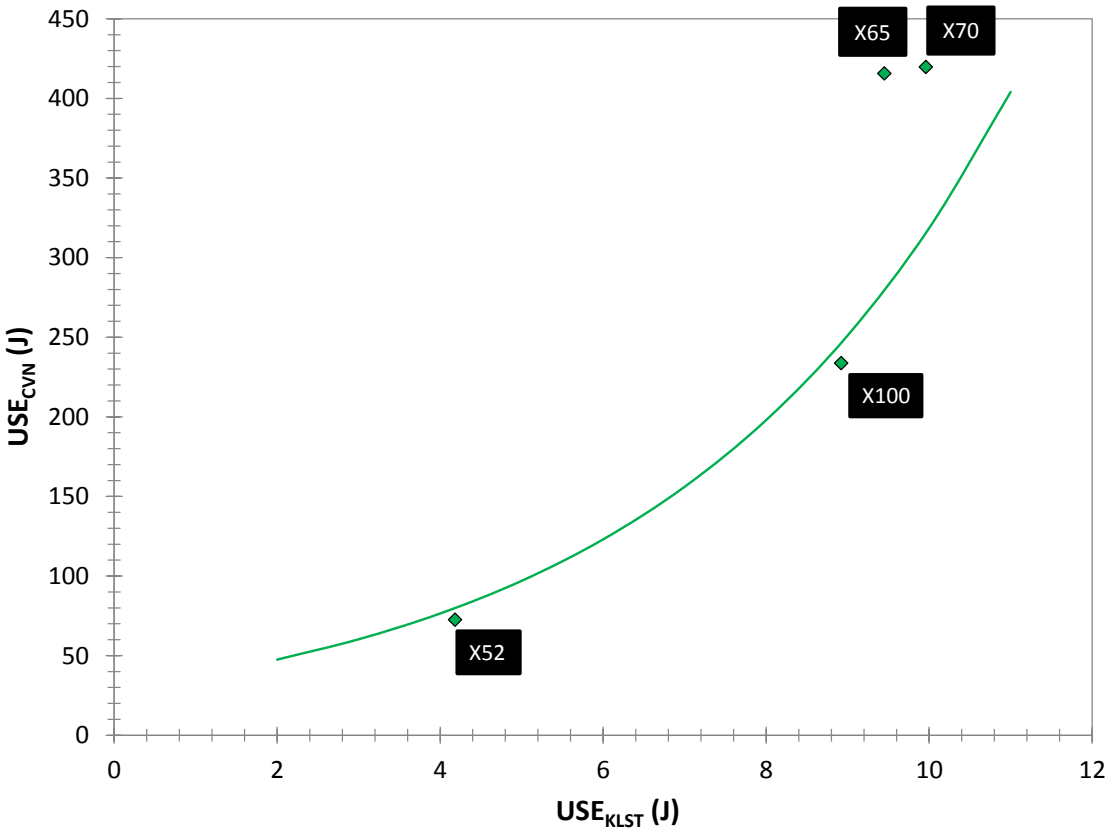

Fig. 15 - Comparison between eq. (12) and NIST results from CVN and KLST tests of line pipe steels